Mathematical Geology, Vol. 38, No. 2, February 2006 (© 2006)
DOI: 10.1007/s11004-005-9011-y

Quantitative Analysis of Porosity Heterogeneity: Application of Geostatistics to Borehole Images[1]

Peter G. Tilke,[2] David Allen,[3] and Asbjorn Gyllensten[4]

High levels of heterogeneity in many carbonate reservoirs have raised concerns about the validity and relevance of small-scale measurements from core plugs and high-resolution logs. While the measurements themselves may be accurate, they may not be representative of the average formation properties. A related question is one of reconciling the measurements made in small volume of investigation data (e.g., core plugs), with the measurements from relatively large volume of investigation data (e.g., wireline logs). This paper presents a technique to quantitatively describe the porosity heterogeneity in a borehole at the scale of several tenths of an inch. The method involves treating high-resolution borehole imagery as a 2D sample from a 3D data volume, and applying geostatistical analysis to these data. We compute the experimental semi-variogram and upscale its range *and* sill *to larger (several inches) scales of measurement to predict the impact of heterogeneity on conventional core plug and logging tool porosity measurements. The resulting dispersion variance between the different measurement scales support the interpretation, application and comparison of these porosity measurements. This technique was applied to an Early Cretaceous carbonate reservoir in Abu Dhabi. We found that the scale of the heterogeneity is typically less than 1– 2in., so that while significant heterogeneity is observed at the core plug and smaller scales of measurement, the larger-volume logging tool measurements smooth out the heterogeneity and show considerably less variability. The differences between porosity measured in core plugs can be completely accounted for by this upscaling effect.*

KEY WORDS: borehole; carbonate; electrical imagery; geostatistics; heterogeneity; image analysis; porosity.

INTRODUCTION

A common challenge in petrophysics and geology is to determine the relevance and reliability of measurements of rock properties such as porosity made at the borehole scale with the same property at the reservoir scale. This challenge is particularly apparent in heterogeneous carbonates.

[1]Received 15 March 2004; accepted 10 May 2005; Published online: 16 May 2006.
[2]Schlumberger-Doll Research, 320 Bent St, Cambridge, Massachusetts, 02141; e-mail: tilke@slb.com.
[3]Schlumberger-Doll Research, 36 Old Quarry Rd, Ridgefield, Connecticut, 06877, USA.
[4]Abu Dhabi Company for Onshore Oil Operations (ADCO), P.O. Box 270, Abu Dhabi, UAE.

Published studies have emphasized the widespread impact of heterogeneity on the rock properties of certain carbonate reservoirs. The results presented in this paper are based on a well in an Aptian field in Abu Dhabi (Russell and others, 2002). In this field, numerous small-scale accurate measurements were made in the laboratory on core plugs. However, because of heterogeneity it was unclear how these measurements were related to the mean formation properties.

A related question is one of reconciling the variability seen in high-resolution (small volume of investigation) measurements (e.g., core plug), with the variability in relatively low-resolution (large volume of investigation) measurements (e.g., wireline log).

The effect of heterogeneity on core plug measurements is illustrated in Figures 1 and 2. Figure 1 illustrates a hand sample from a homogeneous limestone. Porosity measurements made at different locations in this sample would yield very consistent results. Figure 2, in contrast, illustrates a hand sample from a heterogeneous limestone. Porosity measurements from different parts of this sample would show very high variance.

Figure 1 illustrates how a homogeneous formation will yield a narrow range in measured porosity, while a relatively heterogeneous formation (Fig. 2) will yield a wide range of measured porosity.

On the other hand, log measurements which average over a large volume, yield relatively smooth measurements even over intervals in which the core indicates significant heterogeneity (Fig. 3). If the measurement volume of these different observations is correctly accounted for, then the analysis of dispersion variance described in this paper will allow us to quantitatively reconcile these two seemingly inconsistent observations.

QUANTITATIVE HETEROGENEITY ANALYSIS FROM IMAGE DATA

The primary objective of this study is to use high-resolution borehole imagery (Ekstrom and others, 1986; Safinya and others, 1991) to quantitatively describe the porosity heterogeneity in the borehole at the scale of the imaging measurements. The observed heterogeneity is then upscaled to core plug and logging tool measurement scales to reconcile differences observed by these different measurements. Conventional logs are then generated of the predicted heterogeneity at these larger scales of measurement.

The workflow to generate these heterogeneity logs involves the following steps:

1. Start from a borehole image: a 2D array of measurements “on” the borehole wall. Compute the 3D coordinates of each measurement from the hole and tool geometry, and the tool orientation.

Figure 1. Photograph of hand sample of homogeneous limestone.

2. For a given depth, identify all possible two-point pairs of measurements and the chord lengths between them (lags).
3. Assign measurement pairs to bins representing similar lags.
4. Transform the measurement values to a relevant physical property as desired. For instance, image resistivity (R) values may be transformed to porosity (Φ) values. Other possibilities include segmenting the image using new or existing image analysis techniques (e.g., Ibanez and Schroeder, 2003).
5. At each depth in the well, compute the experimental semi-variogram by computing the porosity variance as a function of lag.
6. Derive a model semi-variogram from the experimental semi-variogram for each frame, thereby determining the modeled geostatistical parameters and making them available for further processing or display.
7. From the geostatistical parameters which have been modeled at the scale of the input image measurement, compute the same parameters for measurements with larger volumes of investigation using upscaling approaches.
8. The up-scaled geostatistical model parameters can then be used to generate dispersion variance logs for corresponding core and well log measurements.

Figure 2. Photograph of hand sample of heterogeneous limestone. Some portions of the sample have very low porosity, while other portions are composed of empty vugs.

These steps are described in greater detail in the following sections.

Compute Three-Dimensional Measurement Geometry

Borehole imaging tools produce images of the measured parameter (resistivity, acoustic impedance, density, etc.) on the rock face. At a given depth, the exact 3D coordinate of each image measurement is therefore a function of the hole orientation and shape and the imaging tool configuration.

We use here data from an electrical resistivity imaging tool (Safinya and others, 1991). The tool consists of four pairs of pads and flaps (Fig. 4). The four arms of the tool expand in the borehole so that the pads and flaps press against the rock face. Each pad and flap has 24 resistivity sensors arranged in two horizontal rows of 12 sensors with a horizontal (azimuthal) sensor spacing of 0.2 in. The two rows are placed on top of each other and are azimuthally shifted 0.1 in. with respect to each other giving an effective horizontal spacing of 0.1 in.

As the tool is pulled up the borehole, a measurement is made every 0.1 in. The resulting image consists of 192 (8×24) measurements around the borehole circumference with a vertical sample spacing of 0.1 in. Because the arms press against the borehole wall, the spacing between pads and flaps on different arms is

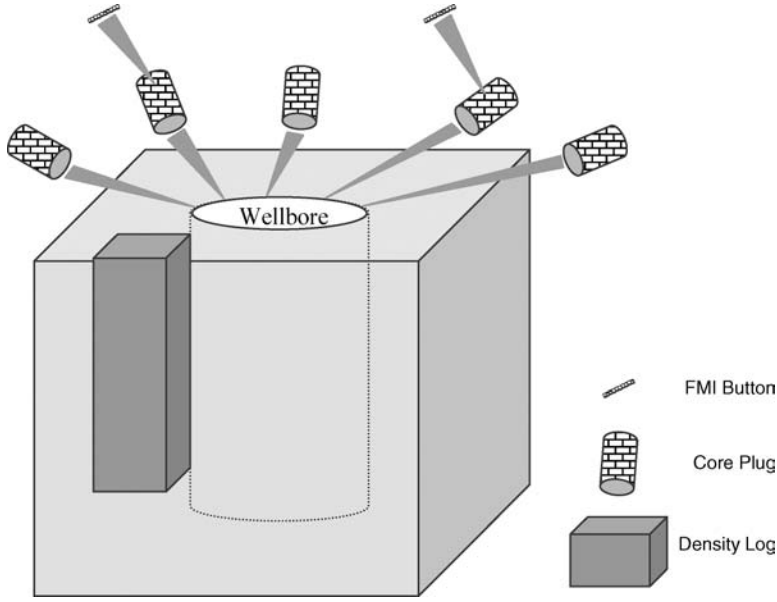

Figure 3. Conceptual diagram illustrating the relative volumes of resistivity image measurements, core plugs, and a density tool. A porosity measurement taken with the density tool would read the average of numerous core plugs, and thereby have a smaller variance than the core plugs, while an image measurement would reveal more variance than the core plug measurements.

a function of the hole diameter. For example, in an 8 in. hole the effective image coverage is about 80% of the circumference, while in an 8.5 in. hole it is about 72% (Fig. 5).

As part of acquiring the image measurements, the orientation of the borehole, the azimuthal orientation of the tool, and the diameter of the hole are all recorded. From this information, the three-dimensional position of every measurement can be derived (Fig. 5). The examples in this document are taken from a vertical well of constant diameter (8.5 in.), which simplifies the analysis slightly.

For a two-point geostatistical analysis, measurement pairs must be identified. While geostatistical theory fully supports the three-dimensional vector analysis, we restrict here our analysis to the measurements at a single depth, ignore the azimuthal orientation of the vectors between the measurements, and only consider their magnitude. The full three-dimensional analysis is a straightforward extension of this reduced approach.

As noted above, there are 192 measurements per depth in the image tool. As such, there are $(192 \times 191)/2 = 18,336$ possible measurement pairs. Once the 3D coordinate of each measurement is known, the horizontal distance between

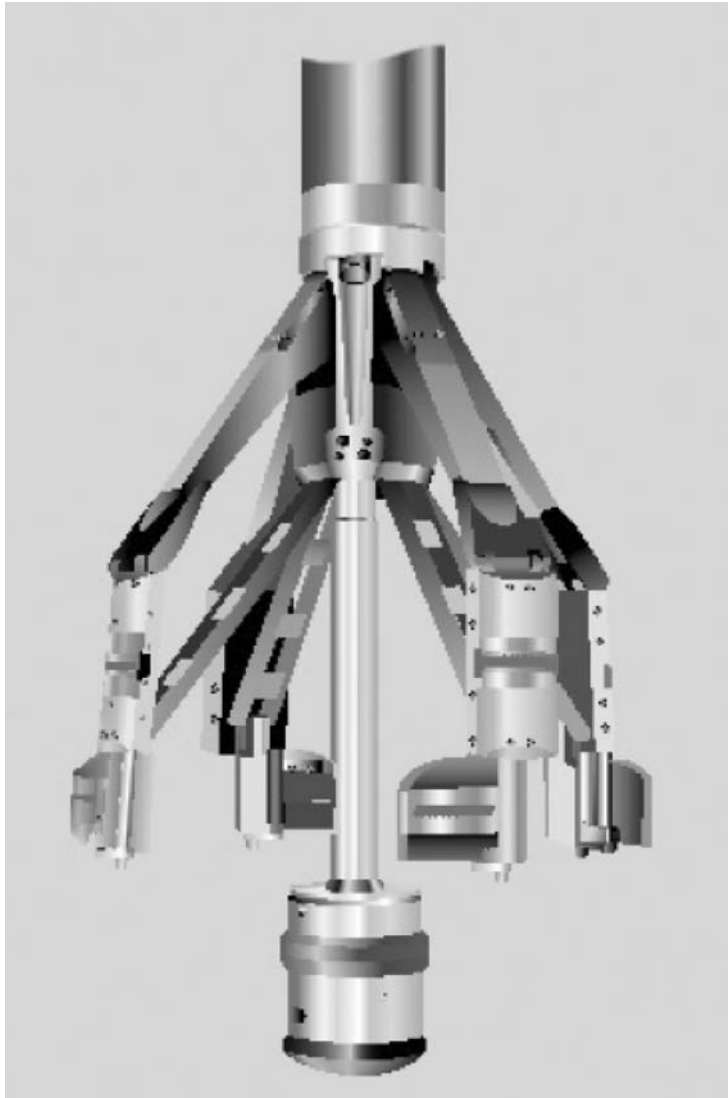

Figure 4. Resistivity image tool illustrating the four pairs of pads and flaps generating 192 measurements per depth.

each measurement pair (L) may be calculated (Fig. 5):

$$L = 2R\sin(\theta/2) \tag{1}$$

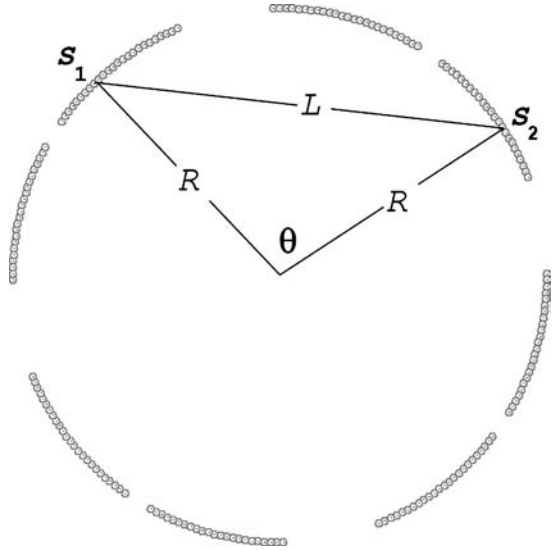

Figure 5. Borehole cross-section illustrating distribution of resistivity image measurements at a given depth. The 192 measurements are distributed across the four pads and four flaps (24 measurements on each). The distance between measurements S_1 and S_2 is given by $L = 2R\sin(\theta/2)$, where θ and R are known from the tool and hole geometry.

We assume here that the heterogeneity is at least locally isotropic in three dimensions, in particular, that there is no vertical variation in formation properties over scales less than several inches. This assumption fails in the presence of bed boundaries. Fortunately, this is not a common occurrence in the studied borehole.

Assign Image Measurement Pairs to Bins with Similar Lags

Geostatistical analysis of the image measurement pairs requires grouping the pairs into bins with similar horizontal lags (L). Selection of the appropriate bin size is an important step. We want the maximum number of bins possible in order to achieve maximum resolution of the semi-variogram structure, but too small a bin size will result in aliasing (e.g., Bloomfield, 2000). The correct minimum bin size is also the effective resolution of the imaging tool (Safinya and others, 1991) dictated by the *Nyquist* Frequency which is twice the measurement spacing (0.1 in.), i.e., 0.2 in. For our 8.5 in. diameter hole example, this results in 43 bins of equal size (except the last which is 0.1 inches). Because of the measurement

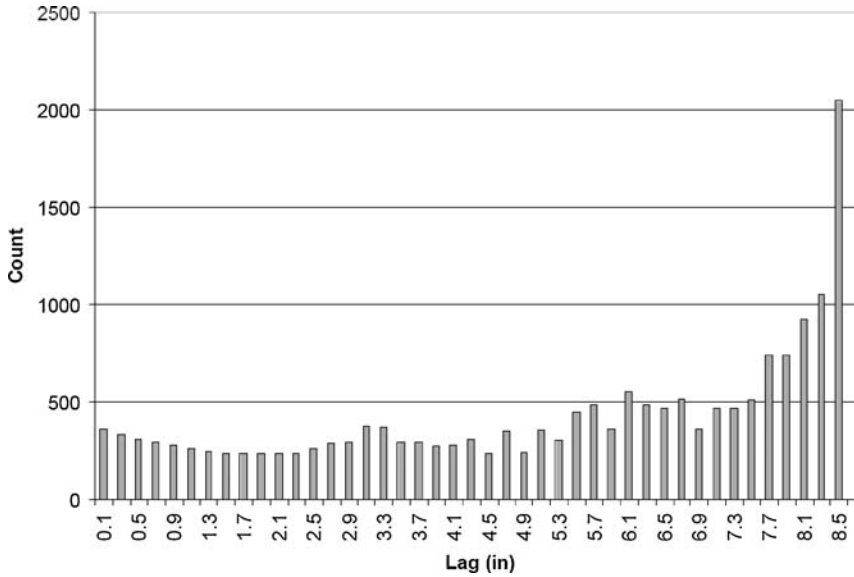

Figure 6. Histogram illustrating frequency of measurement pairs per 0.2 in. sampling bin for 8.5 in. diameter hole. Bin 1 is 0.0–0.2 in., Bin 2 is 0.2–0.4 in., etc.

geometry illustrated in Figure 5, the number of measurements in each of the 43 bins is not uniform (Fig. 6).

As noted earlier, in an 8.5 in. borehole, the imaging tool achieves approximately 72% coverage of the hole circumference. As illustrated in Figure 6, this high coverage results in good bin sampling for every lag distance from 0.1 to 8.5 in. An older generation imaging tool with larger sampling gaps between the pads (e.g., Ekstrom and others, 1986), would yield gaps in the semi-variogram which would reduce the quality of the interpretation.

Transform Resistivity Image to Porosity Image

Once the measurement pairs and bins have been identified, it is necessary to map the resistivity image to a geological or petrophysical property, so that this property can be analyzed in a geostatistical sense. It is possible to use any attribute extracted from the resistivity image. We will transform here the resistivity image to a porosity image.

The recognition that borehole images can be mapped to petrophysical properties is well understood (e.g., Delhomme and others, 1996; Newberry, Grace, and Stief, 1996). Perhaps the best established transformation is that from resistivity

to porosity space using the classic Archie saturation equation (e.g., Fanchi, 2002, p. 61):

$$S_{\mathrm{w}}^{n} = \frac{a R_{\mathrm{mf}}}{\Phi^{m} R} \tag{2}$$

where S_{w} is the saturation of the wetting phase, n is the saturation exponent, a depends on the tortuosity, R_{mf} is the resistivity of the mud filtrate, Φ is the porosity where the measurement is made, m is the cementation exponent, and R is the resistivity of the flushed zone where the measurement is made. This relationship can be rearranged in terms of

$$\Phi = \left(\frac{a R_{\mathrm{mf}}}{S_{\mathrm{w}}^{n} R} \right)^{\frac{1}{m}} \tag{3}$$

Equation (3) may also be written as

$$\Phi = \lambda \, R^{-\frac{1}{m}} \tag{4}$$

where

$$\lambda = \left(\frac{a R_{\mathrm{mf}}}{S_{\mathrm{w}}^{n}} \right)^{\frac{1}{m}} \tag{5}$$

If we assume that λ is constant for a given depth, then we can use Eq. (4) to express the *mean* porosity $\langle \Phi \rangle$ for a given depth as

$$\langle \Phi \rangle = \lambda \left\langle R^{-\frac{1}{m}} \right\rangle \tag{6}$$

where $\langle \, \rangle$ denotes the *expectation* or *mean* of the enclosed. Thus, $\langle R^{-\frac{1}{m}} \rangle$ represents the mean value of $R^{-\frac{1}{m}}$ at the given depth, and is obtained from the 192 resistivity measurements.

Finally, $\langle \Phi \rangle$ may be measured independently using a conventional porosity logging tool (e.g., Ellis, 2003; Luthi, 2001). This allows us to combine Eqs.(4) and (6) to eliminate λ yielding

$$\Phi = \langle \Phi \rangle \frac{R^{-\frac{1}{m}}}{\left\langle R^{-\frac{1}{m}} \right\rangle} \tag{7}$$

Note that we still need to supply the cementation exponent m, which can be obtained from laboratory core measurements (e.g., Ragland, 2002). In this study, m was 2.0 for the entire interval of investigation, within measurement uncertainty.

Compute Experimental Semi-Variogram

Now that we have the porosity image and bins defined, we can compute the sample porosity (Φ) variance $\bar{\gamma}_\Phi(h)$ for each bin (having lag h) with the classic experimental semi-variogram equation

$$\bar{\gamma}_\Phi(h) = \frac{\sum_{i=1}^{n} \left(\Phi_{p(i)+h} - \Phi_{p(i)}\right)^2}{2\,n} \tag{8}$$

where $\Phi_{p(i)+h}$ denotes the porosity at a point distance h from the ith point $p(i)$, and n is the total number of pairs of measurements separated by distance h. A semi-variogram created by this technique is illustrated in Figure 7.

Model Semi-Variogram

For the purposes of this analysis, a simple exponential semi-variogram model (e.g., Journel and Huijbregts, 1978, p. 163) has been defined to fit the experimental data from Equation (8):

$$\gamma_\Phi(h) = C_0 + C_1 \left(1 - e^{-\frac{h}{L_1}}\right) \tag{9}$$

where $\gamma_\Phi(h)$ is the model variance at lag h, C_0 is the *nugget effect*, C_1 the *sill*, and L_1 the *correlation length* or *range* (Journel and Huijbregts, 1978 , p. 163).

To fit the model semi-variogram of Equation (9) to the experimental semi-variogram of Equation (8), the method of Zhang, Van Eijkeren, and Heemink (1995) produced satisfactory results. This technique involves minimizing the cost criterion J (λ), given by

$$J(\lambda) = \sum_{i=1}^{k} \frac{N_{h_i}}{h_i^2} \left[\bar{\gamma}_\Phi(h_i) - \gamma_\Phi(h_i)\right]^2 \tag{10}$$

where i is the bin index, h_i is the lag of the ith bin, and N_{h_i} is the number of sample pairs in the ith bin.

In Figure 7, the resulting model semi-variogram is plotted along with the experimental semi-variogram. We can repeat this analysis for every depth with

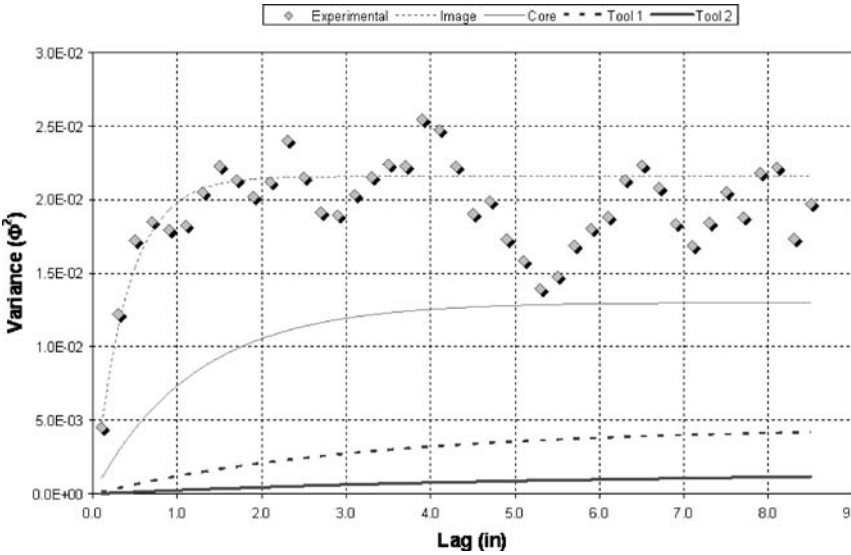

Figure 7. Horizontal semi-variogram for the heterogeneous interval displayed in the middle of interval Figure 11. Superimposed on the experimental data obtained from the porosity image, are model variograms for the resistivity image, core plug, high-resolution tool (Tool 1), and low-resolution tool (Tool 2) (see Table 1). In the experimental data, note the sill with $\Phi^2 = 0.022$ ($\Phi = 14.8\%$) reached at a practical range of approximately 1.2 in. Applying the dispersion analysis described in Equation (19) to the core measurement relative to the larger Tool 2 volume yields $D^2 = 0.0044\,(D = 6.7\%)$. Thus, core plug measurements of porosity would thus be expected to show a 1σ dispersion of $\pm 6.7\%$ if sampled repeatedly at this depth.

imagery in the borehole. The resulting vectors of C_0, C_1, and L_1 can then be plotted as conventional logs. An example is illustrated in the bottom trace of Figure 8.

Upscaling

Now that we have a model for the experimental semi-variogram observed at the small (resistivity image) scale, we are in a position to upscale the model to samples with larger volumes of investigation (e.g., core plugs).

In addition to the image and core plug measurement volumes, we have also considered in this analysis two logging tool measurement volumes corresponding to a high resolution and low resolution porosity tool. The idealized dimensions of these various measurement volumes are listed in Table 1.

If we consider two finite volumes of investigation v (the small image measurement volume at which the experimental semi-variogram was derived) and V (the relatively large core plug or logging tool volume), then we would like to derive

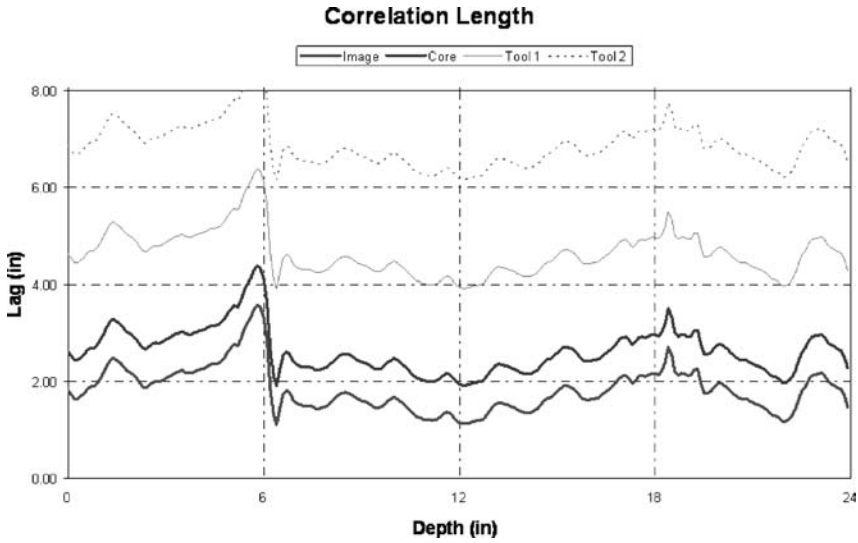

Figure 8. Log of modeled practical range L as a function of depth in the borehole. This log spans 24 in. depth and is centered on the middle of the interval displayed in Figure 11 (top to the left). Note the increase in range from resistivity image tool → core plug → high-resolution tool (Tool 1) → low-resolution tool (Tool 2) as expected from Equation (12). Also note the jump in range at a depth of about 6 in. which is the contact between the homogeneous zone above and the heterogeneous zone below.

the geostatistical parameters for V (i.e., $C_{0,V}$, $C_{1,V}$, and $L_{1,V}$) from the modeled geostatistical parameters for v (i.e., $C_{0,v}$, $C_{1,v}$, and $L_{1,v}$).

To upscale the nugget effect $C_{0,v}$ in Equation (9) it can be shown (Journel and Huijbregts, 1978, p. 156)

$$C_{0,V} = C_{0,v}\frac{v}{V} \tag{11}$$

It can also be shown (Frykman and Deutsch, 1999) that the range L_1 in Equation (9) increases as a function of the increase in volume size, viz.

$$L_{1,V} = L_{1,v} + |V| - |v| \tag{12}$$

Table 1. Dimensions of Idealized Measurement Values

Measurement	Width (in.)	Height (in.)	Depth (in.)	Volume (in.^{3})	Volume (*relative*)
Image tool	0.2	0.2	0.2	0.008	1×
Core plug	1.0	1.0	1.0	1.0	125×
High-resolution tool	3.0	3.0	3.0	27.0	3,375×
Low-resolution tool	3.0	12.0	4.0	144.0	18,000×

where $|V|$ and $|v|$ are the dimensions (lengths) of the volumes V and v in the direction of L_1. As we are not considering direction in this analysis, $|V|$ and $|v|$ become $\sqrt[3]{V}$ and $\sqrt[3]{v}$, respectively.

Finally, to upscale the modeled sill in Equation (9), we must introduce the concept of the point scale sill C_p (Journel and Huijbregts, 1978, p. 77). C_p is defined as the sill for an infinitesimally small volume of investigation. Then, for the small finite volume v, we can define the decrease in sill as follows:

$$C_p - C_v = C_p\overline{\Gamma_v} \tag{13}$$

where $C_p\overline{\Gamma_v}$ is the point-scale sill within the volume v, and $\overline{\Gamma_v}$ is the normalized point-scale sill in v defined below in Equation (16).

Similarly, the decrease in sill for the large volume V can be expressed as

$$C_p - C_V = C_p\overline{\Gamma_V} \tag{14}$$

Equations (13) and (14) are then combined to eliminate the point scale sill C_p yielding the following definition for C_V:

$$C_V = C_v\frac{1-\overline{\Gamma_V}}{1-\overline{\Gamma_v}} \tag{15}$$

The normalized point-scale sill in v is obtained from the double volume integral:

$$\overline{\Gamma_v} = \frac{1}{v^2}\iint \Gamma_p(|\overline{a}-\overline{b}|)\,da\,db \tag{16}$$

where $|\overline{a}-\overline{b}|$ is the Euclidean distance between points a and b, and Γ_p is the normalized point-scale model semi-variogram expressed as

$$\Gamma_p(|\overline{a}-\overline{b}|) = 1 - e^{-\frac{|\overline{a}-\overline{b}|}{L_{1,v}-|v|}} \tag{17}$$

where $L_{1,v} - |v|$ is the modeled point scale range from Equation (9).

Similarly, $\overline{\Gamma_V}$ is expressed as

$$\overline{\Gamma_V} = \frac{1}{V^2}\iint \Gamma_p(|\overline{a}-\overline{b}|)\,da\,db \tag{18}$$

These upscaled geostatistical parameters (Eqs. (11), (12), (15) and (18)) for each of the volumes in Table 1 are then computed for every depth in the borehole. Like

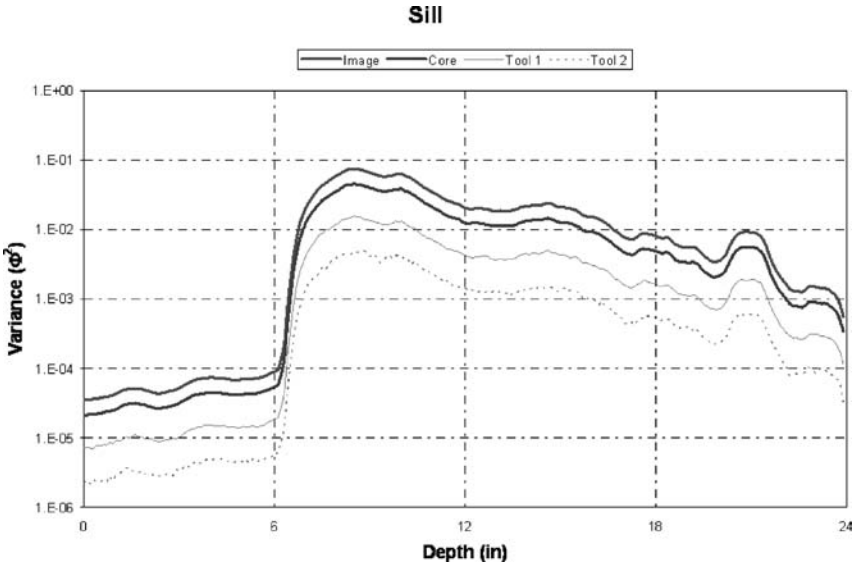

Figure 9. Log of modeled sill C as a function of depth in the borehole. This log also spans 24 in. depth and is centered on the middle of the interval displayed in Figure 11. Note the decrease in sill from resistivity image tool → core plug → high-resolution tool (Tool 1) → low-resolution tool (Tool 2) as expected from Equation (15). Note how this log illustrates the extreme difference in heterogeneity as indicated by the change in magnitude of the sill at the 6 in. depth.

the parameters for the image scale (Eq. (9)), the upscaled parameters may also be plotted as conventional well logs (Figs. 8 and 9).

Construct Dispersion Variance Logs for Porosity Measurements

Dispersion variance may be defined as the variance of an observation made at a small volume v within a larger volume V (Journel and Huijbregts, 1978, p. 61). The dispersion variance of Φ may then be expressed in terms of the mean values of the variances (Journel and Huijbregts, 1978 , p. 67) as

$$D_{\Phi}^{2}(v|V) = \bar{\gamma}_{\Phi}(V, V) - \bar{\gamma}_{\Phi}(v, v) \tag{19}$$

where $\bar{\gamma}_{\Phi}(v, v)$ is the mean variance of Φ over the volume v (Journel and Huijbregts, 1978, p. 54), and may be expressed in terms of the geostatistical parameters for v:

$$\bar{\gamma}_{\Phi}(v, v) = C_{0,v} + C_{1,v}\overline{\Gamma_{v}} \tag{20}$$

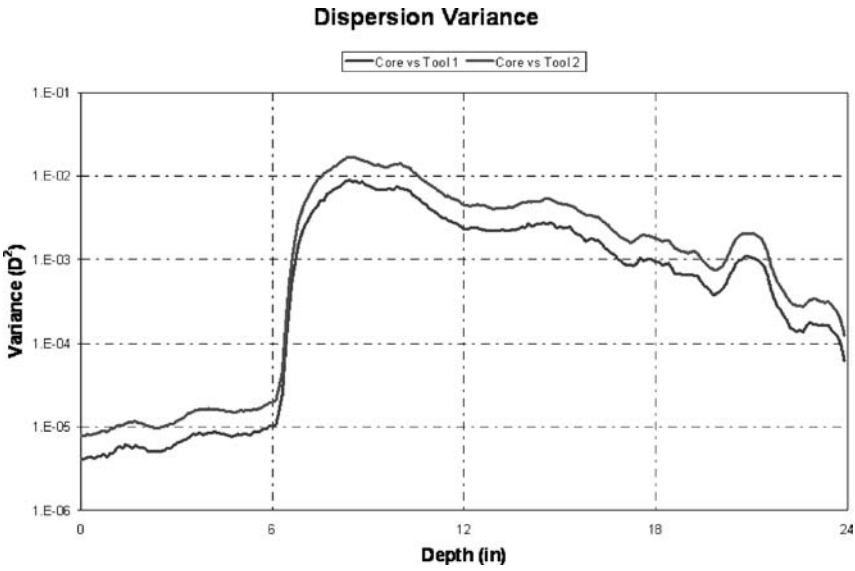

Figure 10. Log of modeled dispersion variance D^2 as a function of depth in the borehole. Like Figures 8 and 9, this log corresponds to the depth range displayed in Figure 7. Here the dispersion variance is computed from Equation (19) with the small volume (v) being the core plug volume (Table 1), and the large volume (V) being either the Tool 1 or Tool 2 volumes (Table 1). Again, note the large change in dispersion from the shallow homogeneous zone above 6 in., and the deeper heterogeneous zone below 6 in. In the heterogeneous zone at a depth of 12 in. $D^2 = 0.0044$ ($D = 6.7\%$) for core vs. Tool 2, while in the homogeneous zone at a depth of 3 in. $D^2 = 0.00001$ ($D = 0.25\%$). A hand sample in the heterogeneous zone would resemble Figure 2, while the homogenous zone might resemble Figure 1.

Similarly,

$$\bar{\gamma}_\Phi(V, V) = C_{0,V} + C_{1,V}\,\overline{\Gamma_V} \tag{21}$$

Thus, Equations (19)–(21)allow us to compute the dispersion variance for all our idealized volumes (Table 1) at every imaged depth in the well. This is illustrated by the example dispersion variance log in Figure 10. Note that this interval straddles a homogeneous interval above and a heterogeneous one below.

DISCUSSION

Figure 11 illustrates a section of the reservoir having moderate porosity (22%). This 24 in. high interval is characterized by a homogeneous layer in the top 6 in. in sharp contact with a heterogeneous layer below. This can be seen

Figure 11. Porosity image of 24 in. high interval around the 26.7 in. circumference ($8.5 \times \pi$) of the borehole. The horizontal grid lines have a vertical spacing of 6 in. Note the relatively large gaps between the four arms, and the relatively small gap between each pad-flap pair. The mean porosity of the interval is 22%. *Black* is relatively high porosity, while *white* indicates relatively low porosity. Note the very heterogeneous layer in the middle of the image comprising numerous 1–2 in. diameter vugs. Also note the abrupt contact above with a relatively homogeneous layer.

clearly in the image log but also in the dispersion variance log (Fig. 10). The semivariogram for the heterogeneous section (Fig. 7) illustrates a practical range of 1.2 in. corresponding visually to the mean size of the vugs in this interval (Fig. 11). The image (Fig. 11) also suggests that the heterogeneity decreases gradually in the bottom 18 in. of the interval as one goes deeper. This is supported by the gradual decrease in dispersion variance over the interval 9–24 in. (Fig. 10). A semivariogram from the top of the homogeneous interval is presented in Figure 12. The variogram indicates a somewhat longer practical range of 1.8 in., but the sill is dramatically lower than in Figure 7 reflecting the homogeneity.

A comparison of the predicted heterogeneity at the core plug scale of measurement with actual core plug porosity measurements is illustrated in Figure 13. This figure illustrates a 70 ft depth interval where the shallower section (0–31 ft) is heterogeneous, and the deeper section (31–70 ft) is homogeneous. There are

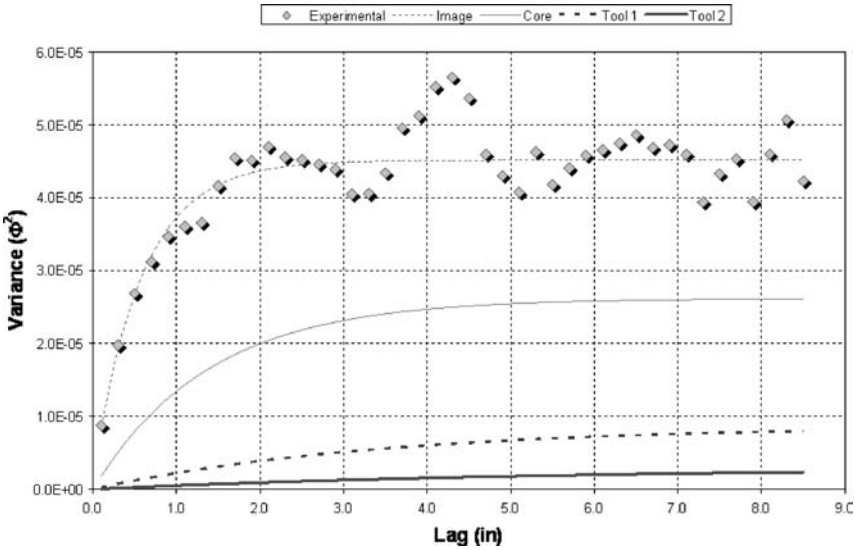

Figure 12. Horizontal semi-variogram for the homogeneous interval displayed in the top of the interval illustrated in Figure 11. Compare this variogram with the one for the heterogeneous interval (Figure 7). In the experimental data, note the sill with $\Phi^2 = 0.00004$ ($\Phi = 0.6\%$) reached at a practical range of approximately 1.8 in. Applying the dispersion analysis described in Equation (19) to the core measurement relative to the larger Tool 2 volume yields $D^2 = 0.00001$ ($D = 0.2\%$). Thus, core plug measurements of porosity would be expected to show virtually no dispersion if sampled repeatedly at this depth.

three logs in this interval: the mean porosity as measured with the porosity tool, and the $\pm 2\sigma$ modeled dispersion logs around the mean porosity. Also illustrated in this figure are core plug porosity measurements made in the laboratory. In the heterogeneous section, the high degree of heterogeneity is illustrated by both the $\pm 2\sigma$ dispersion logs and the dispersion (scatter) in the core plug measurements. In the homogeneous section, the dispersion logs and the core plugs are consistent in that they both illustrate significantly less dispersion. Note that in the homogeneous interval there is an obvious shift to higher porosity of about 2–3% observed in the core plug measurements. A likely source of this inconsistency is biased sampling of the core plugs. In both the heterogeneous and homogenous intervals, the predicted and observed core plug dispersion is remarkably consistent. Therefore, if one corrects for discrepancies introduced by biased sampling of the core plugs, the apparent discrepancy in the relatively uniform porosity measured by the porosity tool and the wide dispersion measured by the core plugs in the heterogeneous intervals can be explained by heterogeneity.

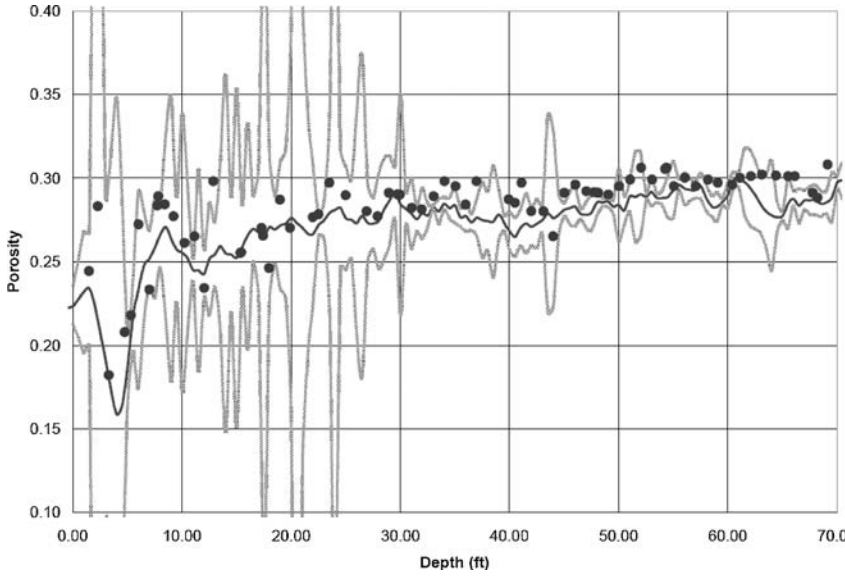

Figure 13. Composite porosity log displaying logging tool porosity (heavy curve) with core plug porosity (circle points). Also displayed (light curves) is the $\pm 2\sigma$ dispersion "envelope" around the logging tool porosity. Two features are of note here: (1) As predicted by this technique, approximately 2σ of the core plug measurements fall within the dispersion "envelope."(2) The log straddles a heterogeneous zone above (0–31 ft), and a homogeneous zone below (31–70 ft). The differences in heterogeneity between the two zones are reflected in both the dispersion "log," and the core plug measurements.

CONCLUSIONS

Understanding heterogeneity is particularly important for understanding fluid flow behavior in carbonates. The heterogeneity observed in carbonates at the resolution of borehole imaging tools is typically related to the presence of macro or vuggy porosity in a matrix characterized by interparticle porosity (Lucia, 1999, p. 25). While the presence of vugs will increase the porosity of the rock, unless these vugs are interconnected or "touching," they will have no effect on the overall permeability, and the resulting permeability will be driven by the interparticle porosity of the matrix (Lucia, 1999, p. 30). Thus, when modeling the fluid flow behavior at the reservoir scale, it is crucial to understand not only the magnitude of the porosity, but also its nature and resulting heterogeneity as observed at the borehole scale.

In this paper, we have demonstrated that geostatistical analysis can be applied to borehole image data in order to generate an improved understanding of formation heterogeneity. Specifically, we have demonstrated how to

1. generate an experimental semi-variogram from high resolution imagery for every imaged depth;
2. extract model parameters from the experimental semi-variograms;
3. upscale the geostatistical model parameters to larger measurement volumes.

We have also shown how the borehole resistivity images can be transformed into porosity values. Further, because the geostatistical approach depends on local porosity differences at a given depth (rather than absolute values), this petrophysical transformation (resistivity to porosity) is very precise.

In our study of the carbonate reservoir from Abu Dhabi, we observed that the scale of the imaged heterogeneity is typically less than 1–2 in. The result is that in heterogeneous intervals, significant dispersion is observed in core plug measurements which have a similar dimension. Wireline log measurements that sample a much larger volume typically "average" out this variability. The differences between porosity measured in core plugs and that measured by wireline logging tools can be completely accounted for by this upscaling effect.

The power of this technique has been recognized and is now being applied to a variety of complex carbonate reservoirs in order to

1. characterize different intervals in terms of their heterogeneity, and
2. explain apparent differences between porosity measurements made with core plugs and logs.

REFERENCES

Bloomfield, P., 2000, Fourier analysis of time series—An introduction: Wiley, New York, 288 p.

Delhomme, J. P., Bedford, J., Colley, N. M., and Kennedy, M. C., 1996, Permeability and porosity upscaling in the near wellbore domain—The contribution of borehole electrical images: Soc. Petrol. Eng., Paper no. 36822, p. 89–101.

Ekstrom, M. P., Dahan, C. A., Chen, M. Y., Lloyd, P. M., and Rossi, D. J., 1986, Formation imaging with microelectrical scanning arrays *in* Proceedings of the SPWLA 27th Annual Logging Symposium, p. 1–21.

Ellis, D. V., 2003, Formation property estimation from density logs: Petrophysics, v. 44, no. 5, p. 306–316.

Fanchi, J. R., 2002, Shared earth modeling—Methodologies for integrated reservoir simulation: Elsevier, New York, 320 p.

Frykman, P., and Deutsch, C. V., 1999, Geostatistical scaling laws applied to core and log data: Soc. Petrol. Eng., Paper no. 56822, p. 1–12.

Ibanez, L., and Schroeder, W., 2003, The ITK software guide—The insight segmentation and registration toolkit: Kitware Inc., Clifton Park, New York, 580 p.

Journel, A. G., and Huijbregts, Ch. J., 1978, Mining geostatistics: Academic Press, New York, 600 p.

Lucia, F. J., 1999, Carbonate reservoir characterization: Springer-Verlag, New York, 226 p.

Luthi, S. M., 2001, Geological well logs: Their use in reservoir modeling: Springer-Verlag, New York, 373 p.

Newberry, B. M., Grace, L. M., and Stief, D. D., 1996, Analysis of carbonate dual porosity systems from borehole electrical images: Soc. Petrol. Eng., Paper no. 35158, p. 1–7.

Ragland, D. A., 2002, Trends in cementation exponents (m) for carbonate pore systems: Petrophysics, v. 43, no. 5, p. 434–446.

Russell, S. D., Akbar, M., Vissapragada, B., and Walkden, G. M., 2002, Rock types and permeability prediction from dipmeter logs—Shuaiba Reservoir (Aptian), Abu Dhabi: Am. Assoc Petrol. Geol. Bull., v. 86, no. 10, p. 1709–1732.

Safinya, K. A., Le Lan, P., Villegas, M., and Cheung, P. S., 1991, Improved formation imaging with extended microelectrical arrays: Soc. Petrol. Eng., Paper no. 22726, p. 653–664.

Zhang, X. F., Van Eijkeren, J. C. H., and Heemink, A. W., 1995, On the weighted least-squares method for fitting a semi-variogram model: Comput. Geosci., v. 21, no. 4, p. 605–608.